Journal of
Micro/Nanolithography,
MEMS, and MOEMS

Nanolithography.SPIEDigitalLibrary.org

Diffraction analysis of digital micromirror device in maskless photolithography system

Zheng Xiong
Hua Liu
Xiangquan Tan
Zhenwu Lu
Cuixia Li
Liwei Song
Zhi Wang

SPIE.

Diffraction analysis of digital micromirror device in maskless photolithography system

Zheng Xiong,[a,b] Hua Liu,[a,*] Xiangquan Tan,[a] Zhenwu Lu,[a] Cuixia Li,[a,b] Liwei Song,[a] and Zhi Wang[a]
[a]Chinese Academy of Sciences, Changchun Institute of Optics, Fine Mechanics and Physics, Changchun 130033, China
[b]University of Chinese Academy of Sciences, Beijing 130039, China

Abstract. A digital micromirror device (DMD) acts as a spatial light modulator in a maskless photolithography system. Illuminated by coherent light, DMD performs as a two-dimensional diffraction grating because of its periodical internal structure. Diffraction efficiency is an important factor for evaluating the exposure doses. A diffraction model of DMD based on Fourier analysis demonstrates that errors of the DMD's manufacture and the precision of the machining of the optical mechanical structure affect the diffraction efficiency. Additionally, analysis of exposure results by the diffraction model of DMD in Tracepro explains the degradation of the exposure quality and is helpful for calibrating the direction of optical focusing. [DOI: 10.1117/1.JMM.13.4.043016]

Keywords: MOEMS; digital micromirror device; blazed grating; diffraction efficiency; spatial light modulator; maskless photolithography system.

Paper 14119 received Aug. 8, 2014; accepted for publication Nov. 7, 2014; published online Dec. 16, 2014.

1 Introduction

A digital micromirror device (DMD), invented by Texas Instruments in 1988, is the large-scale commercial implementation of a micro-optical-electro-mechanical system.[1–3] For the advantages of high contrast ratio, high throughput, and wide dynamic control range, DMD has attracted a great deal of attention in projectors, holographic displays, tunable lasers, and maskless photolithography systems (MPLS).[4–9] In MPLS, DMD replaces the traditional photomask to contribute to the cost-effective production of printed circuit boards and flat liquid crystal panels, by circumventing the expense of fabrication, maintenance, and the process period of the mask.[9]

In MPLS, light sources are generally laser diode or high pressure mercury lamps filtered by a narrow bandpass filter.[8] Because of the periodical configuration and the coherence of the light source, the irradiance of the DMD is influenced by diffraction effects.[10] Evaluation of the diffraction efficiency is used to predict the exposure doses.[9] Even though several researchers have investigated DMD's diffraction, [9–14] there are still several issues which have not been fully understood. For example, errors of the DMD's manufacture and the precision of the machining of the optical mechanical structure influence the diffraction efficiency. A diffraction model of a DMD in optical ray-tracing software, which can directly facilitate the analysis of the exposure results, has not been reported before. In this paper, a numerical model of the DMD's diffraction is established by Fourier analysis and is verified by diffraction measurement. We simulate the effects on the diffraction efficiency caused by the errors, such as the bandwidth of the light source, the micromirror tilt angle variation, the error of the incident angle, and the orientation's error of the micromirror axis of rotation. Additionally, a diffraction model in Tracepro is established according to the results of the diffraction measurement. With this model, we explain the degradation of exposure quality and provide a method to calibrate the direction of optical focusing.

2 Characterization of Diffraction of Digital Micromirror Device

2.1 *Fourier Analysis*

Figure 1[15] presents the diagram of a DMD. A DMD consists of a 1024×768 array of moving micromirrors, which are controlled by underlying complementary metal oxide semiconductor electronics. Each micromirror is $12.68 \times 12.68\ \mu m^2$, mounted on a 13.68 μm pitch, and can be rotated to either a $+12$ deg or -12 deg position along the diagonal direction by the central post with a width of 2 to 3 μm. Each one acts as an on/off switch by reflecting light either toward or away from the optical system. In the general Fourier analysis of a DMD, [11,13,16] a single micromirror is considered as a rectangular function and the micromirror array is considered as a sampling function limited by the input pattern of the DMD. Then, the whole reflection equation for the DMD can be presented as follows:

$$R(x,y) = \left[\mathrm{rect}\left(\frac{x}{a}\right)\mathrm{rect}\left(\frac{y}{a}\right) - \mathrm{rect}\left(\frac{x}{b}\right)\mathrm{rect}\left(\frac{y}{b}\right)\right] \otimes f(x,y)\mathrm{comb}\left(\frac{x}{c}\right)\mathrm{comb}\left(\frac{y}{c}\right), \quad (1)$$

where a is the size of a single micromirror, b is the size of the central post, and c is the pitch size as shown in Fig. 2. $f(x,y)$ represents the input pattern which controls the on/off state of each micromirror.

However, as the micromirrors rotate along their diagonal direction, there is a phase difference between the reset state and the rotated state. This phase difference affects the

*Address all correspondence to: Hua Liu, E-mail: liuhua_rain@aliyun.com

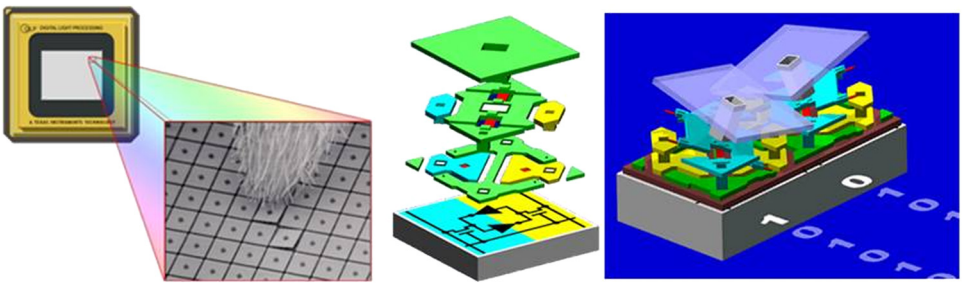

Fig. 1 Diagram of digital micromirror device (DMD).

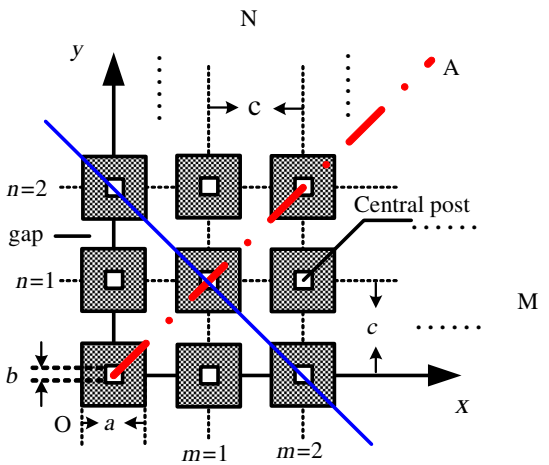

Fig. 2 Diagram of microstructure of DMD.

location of the blazed diffraction order.[9] Thus, it is incomplete that a rectangular function without the phase term is applied for a single micromirror. The phase difference is calculated by an infinitesimal method as follows. Figure 3(a) gives the diagram of a single micromirror. We take an arbitrary small element $dxdy$ as an example. The direction of the incident light is along the diagonal direction OA, which is the diagonal as Fig. 3(b) shows. Considering there is no phase difference among the small elements in a counter-diagonal direction, the phase difference between $dxdy$ and O can be calculated along OA. Figure 3(b) is the diagram of the cross profile of the micromirror along OA. The phase difference is presented as follows:

$$\phi = \frac{2\pi}{\lambda}(\mathrm{OD}\tan w\cos\theta_i + \mathrm{OD}\tan w\cos\theta_r), \tag{2}$$

where Φ is the phase difference, λ is the wavelength of the incident light, θ_i is the incident zenith angle between the incident direction of the beam and the normal direction of the DMD (z direction), and θ_r is the diffracted zenith angle between the diffraction direction of the beam and the normal direction of the DMD.

Including the phase difference Φ in Eq. (1), the whole reflection equation of the DMD is presented as follows:

$$R(x,y) = \left[\mathrm{rect}\left(\frac{x}{a}\right)\mathrm{rect}\left(\frac{y}{a}\right) - \mathrm{rect}\left(\frac{x}{b}\right)\mathrm{rect}\left(\frac{y}{b}\right)\right]\exp(i\phi) \otimes f(x,y)\mathrm{comb}\left(\frac{x}{c}\right)\mathrm{comb}\left(\frac{y}{c}\right). \tag{3}$$

The Fraunhofer diffraction pattern is presented as follows by the Fourier transformation of Eq. (3):

$$U(u,v) = \left\{a^2\,\mathrm{sinc}\left[a\left(u-\frac{\xi}{\sqrt{2}}-u_0\right)\right]\mathrm{sinc}\left[a\left(v-\frac{\xi}{\sqrt{2}}-v_0\right)\right] - b^2\,\mathrm{sinc}\left[b\left(u-\frac{\xi}{\sqrt{2}}-u_0\right)\right]\mathrm{sinc}\left[b\left(v-\frac{\xi}{\sqrt{2}}-v_0\right)\right]\right\} \bullet \sum_{m=0}^{M}\sum_{n=0}^{N} F\left(u-\frac{m}{c}-u_0, v-\frac{n}{c}-v_0\right), \tag{4}$$

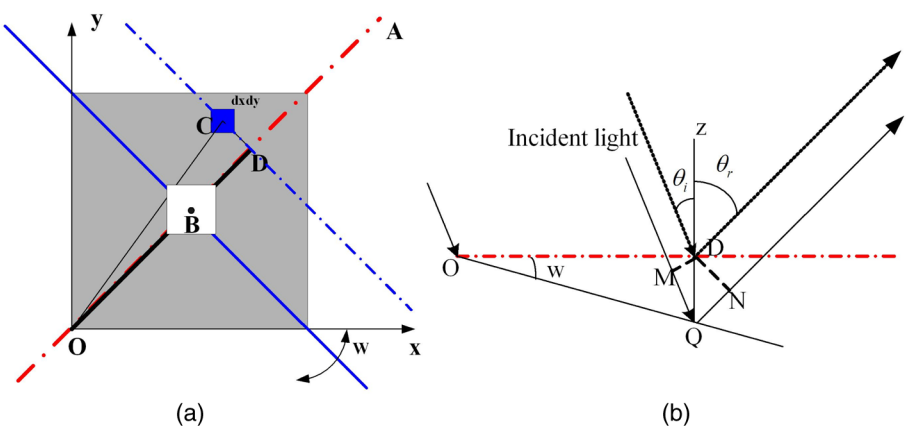

Fig. 3 (a) Diagram of micromirror and (b) cross profile in single micromirror along OA.

where $u = (\sin\theta_r \cos\varphi_r)/\lambda$, $v = (\sin\theta_r \sin\varphi_r)/\lambda$, $u_0 = (\sin\theta_i \cos\varphi_i)/\lambda$, and $v_0 = (\sin\theta_i \sin\varphi_i)/\lambda$. Here, φ_i is the incident azimuth angle between the incident direction of the beam and the x direction, φ_r is the diffraction azimuth angle between the diffraction direction of the beam and the x direction, and M and N are the number of micromirrors along the x and y directions, respectively.

Equation (4) includes two parts. One is a sinc function which represents the diffraction of a single micromirror. Another part is $F(u, v)$ which represents the frequency spectrum of the input pattern $f(x, y)$. If the diffraction pattern of the DMD is observed within the extent of the Fraunhofer diffraction, $f(x, y)$ is duplicated at each diffraction order; this results from the sampling property of the DMD.

2.2 *Verification of Numerical Model of Digital Micromirror Device by Diffraction Measurement*

Based on Eq. (4), we calculate the diffraction efficiency and diffraction angle. They are listed in the simulated results of Table 1. The diffraction measurement is done by the setup as shown in Fig. 4. The light source is a fiber-coupled laser diode with a peak wavelength at 403.2 nm. The beam from the light source is homogenized by an engineering diffuser (ED1-C20, Thorlabs. Inc.), which reshapes the energy distribution of the incident light into a hat-shape within ± 10 deg. Then, with a collimating lens, the light illuminates on the DMD surface within a 5% nonuniformity and ± 2 deg divergence angle. The incident azimuth angle and incident zenith angle are 45 deg and 24 deg, respectively. Then, the diffraction angle is measured using xy and φ stages. The diffraction energy is measured with an optical power meter. The process of measurement is as follows. The φ stage on the DMD is used for measuring the diffraction azimuth angle φ_r. It rotates until the diffraction order is located on the x axis. The rotated angle is the diffraction azimuth angle φ_r. Then, the xy stage on the optical power meter is moved to the position of each diffraction order. The moving distance of the xy stage is the distance between the normal direction of the DMD and the measured diffraction order. The vertical distance, which is between DMD and the optical power meter along the normal direction of DMD, is set as 600 mm before the experiment. The diffraction zenith angle θ_r can be calculated by the arc-tan operation between the vertical distance and the moving distance.

Table 1 gives simulated results and measuring results. There are small deviations between the two results. The deviation of the diffraction efficiency results from stray light in diffraction measurement, and the deviation of the diffraction angle results from the precision of the moving stages.

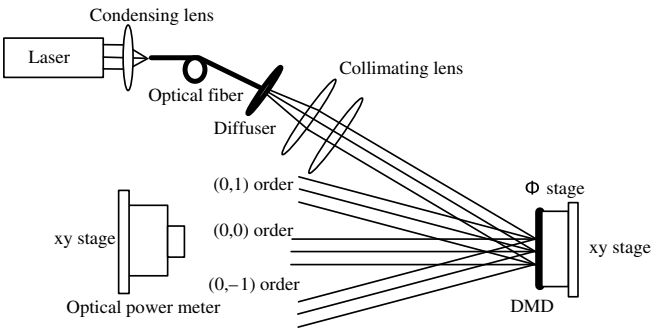

Fig. 4 Schematic of diffraction measurement setup.

2.3 *Diffraction Model in Optical Ray-Tracing Software*

The numerical model of a DMD's diffraction is established and verified with the diffraction measurement. But it is not enough for analysis of the MPLS, because the MPLS is analyzed in optical ray-tracing software such as Tracepro. In Tracepro 7.21, even though there is a model of the DMD which is represented as an array of micromirrors, the diffraction property of the DMD cannot be demonstrated. Therefore, based on the results of Table 1, a diffraction model of the DMD is established.

Considering its property of two-dimensional (2-D) diffraction, the DMD is orthogonally considered as two linear gratings overlapping each other. First, a rectangular board is set to act as the DMD. The board's area is 14×10 mm^2 and its thickness is 1 μm. This size is as the same as that of the DMD. A diffraction property of the grating is established by the user-defined linear grating of Tracepro. The diffraction efficiency of the grating is calculated with the square root of the diffraction efficiency of the DMD in Table 1. Then, the diffraction property of the grating is applied to the front surface of the board along the x direction and to rear surface of the board along the y direction, respectively. In this way, the 2-D diffraction property is obtained which corresponds to the sinc function in Eq. (4). However, the picture input in the DMD is modulated by sampling the DMD and is in every diffraction order. Therefore, in order to demonstrate the DMD's diffraction as being closer to the actual result, a picture board with a fringes pattern is established in mechanical software Unigraphics NX, and is then imported

Table 1 Simulated results and measuring results of diffraction efficiency and diffraction angle.

		Diffraction orders (m, n)				
Items	Items	(0,0)	(1,0) or (0,1)	(−1,0) or (0, −1)	(1,1) or (−1, −1)	(1, −1) or (−1, 1)
Diffraction efficiency	Simulated results	0.5757	0.0926	0.0286	0.0152	0.0048
	Measuring results	0.5558	0.0996	0.0252	0.0096	0.0053
Diffraction angle (φ_r, θ_r)	Simulated results	(45, −0.6844)	(−68.2386, −1.3055)	(77.4849, −2.2338)	(45, −3.0848)	(−29.0765, −2.4954)
	Measuring results	(45.323, −0.593)	(−67.943, −1.333)	(−76.713, −2.193)	(45.183, −2.753)	(−29.643, −2.3830)

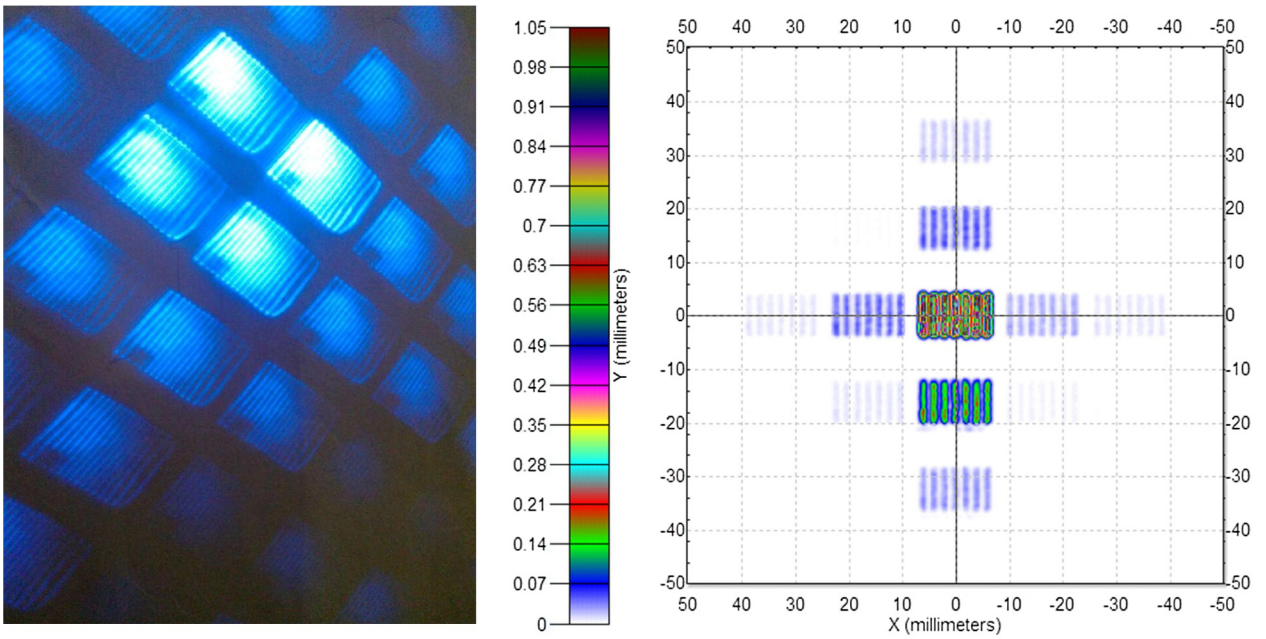

Fig. 5 (a) Experimental result of diffraction distribution and (b) simulated result of the diffraction distribution.

in front of the DMD board of Tracepro. Figure 5(b) gives the simulated results of the DMD's diffraction which is represented as the combination of the rectangular board with the picture board. For verifying the diffraction model's availability, an actual experiment is done using the same setup as Fig. 4. The diffraction pattern is observed at 600 mm which is the same as the distance set in Tracepro. The experimental result is shown in Fig. 5(a). By comparing Fig. 5(a) with Fig. 5(b), the simulated result matches with the experimental result. Therefore, this diffraction model can be used for the analysis of MPLS in next section.

3 Analysis of Diffraction Efficiency with Errors of System Parameters

The diffraction efficiency[9] is a critical parameter which impacts the exposure doses. We analyze the effects of diffraction efficiency caused by errors, such as the error of mirror tilt angle variation, the orientation's error of the micromirror axis of rotation, the error of the incident angle, and the bandwidth of the light source.[17] With Eq. (4), the diffraction efficiency of every diffraction order is determined with the sinc function. The $F(u, v)$ only modulates the image in every diffraction order. Therefore, in this section, the input pattern is set as a white image. It means that $f(x, y)$ is 1 for all micromirrors.

0.7 XGA 12 deg DDR DMD[17] is chosen as the spatial light modulator in our MPLS. From its datasheet, the micromirror tilt angle has an error of ± 1 deg from 11 deg to 13 deg, and the orientation of the micromirror axis of rotation also has an error of ± 1 deg from 44 deg to 45 deg. These are the result of errors in the DMD's manufacture. Figure 6 gives a relationship between the diffraction efficiency of the main order and the angle of the micromirror tilt. The diffraction efficiency changes from a maximum to a minimum as the angle of the micromirror tilt varies from 11 deg to 13 deg. This is because the angle of the micromirror tilt determines the location of the diffraction envelope.[9] Figure 7 gives a relationship between the diffraction efficiency of the main order and the angle of the axis of the rotation. The diffraction efficiency decreases by about 0.03%. The angle's error of axis of rotation has little effect on the diffraction efficiency, because the axis of rotation determines the shift's direction of the diffraction envelope.[9]

Strictly, the laser source used in MPLS has a bandwidth as shown in Fig. 8, which is a spectrogram characterized by a fiber optical spectrometer (AvaSpec-ULS2048) whose spectral resolution is 0.6 nm. The peak wavelength of the laser source is 403.2 nm. The bandwidth at the full width at half maximum is 2 nm. Figure 9 gives the relationship between the diffraction efficiency and the wavelength. From 402.1 to 404.3 nm, the diffraction efficiency linearly decreases by about 10%. This is because the wavelength determines the location of the diffraction envelope.[9] Thus, the energy of the light source should be adjusted according to the average diffraction efficiency within the bandwidth.

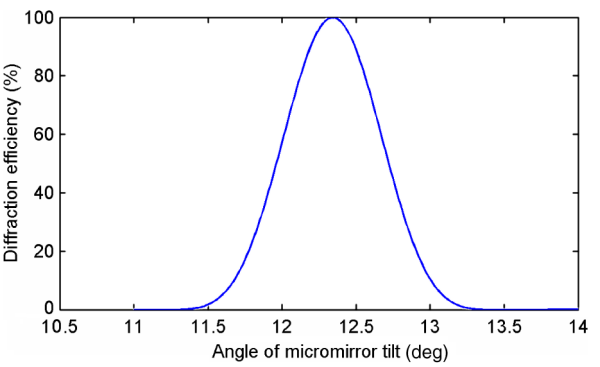

Fig. 6 Calculated diffraction efficiency with the angle of the micromirror tilt.

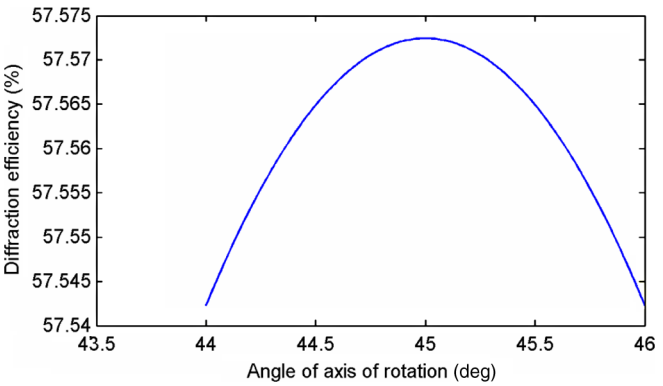

Fig. 7 Calculated diffraction efficiency with the angle of the axis of rotation.

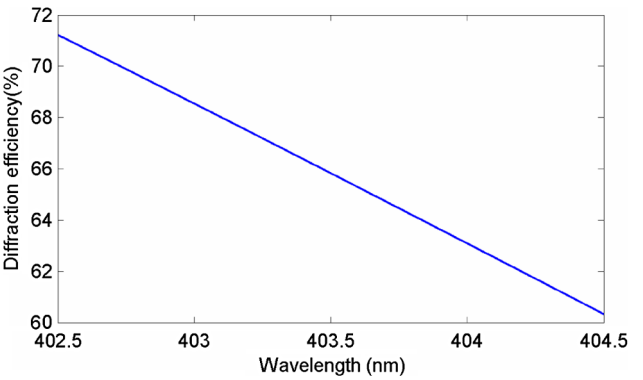

Fig. 9 Calculated diffraction efficiency with the wavelength.

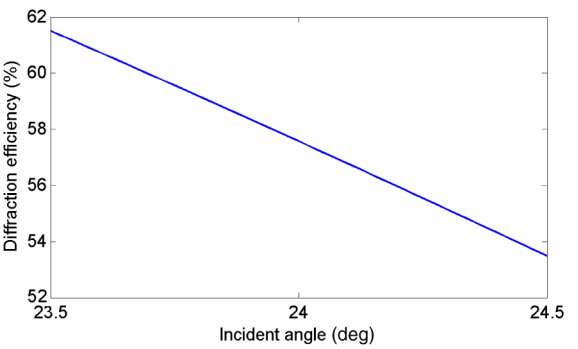

Fig. 10 Calculated diffraction efficiency with the incident angle.

The precision of machining of the optical mechanical structure leads to an error of the incident angle within ± 0.5 deg. Figure 10 gives the relationship between the diffraction efficiency and the incident angle. The diffraction efficiency decreases by about 9%. This is because the incident angle also determines the location of the diffraction envelope[9]. Therefore, the precision of machining of the optical mechanics should be within ± 0.1 deg.

4 Calibration of the Direction of Optical Defocusing by Digital Micromirror Device's Diffraction

The total energy is distributed into every diffraction order according to their diffraction efficiencies. Based on the diffraction angles in Table 1, the projection optics (NA = 0.045) is able to receive the energy of the diffraction orders including (0, 0), (± 1, 0), (0, ± 1), and (± 1, ± 1). Therefore, the energy efficiency of the projection optics is about 82%. However, as the depth of focus is 6.25 μm, the exposure quality is greatly degraded by a small defocusing amount. In this case, it is important to calibrate the direction of the optical focusing. By comparison of the simulated results with the exposure results, we use the diffraction of the DMD to analyze the degradation of the exposure quality. The result of analysis provides a method to calibrate the direction of optical focusing.

Figure 11 is the model of MPLS in Tracepro. The light source is a fiber-coupled laser diode with a peak wavelength at 403.2 nm. In the illumination optics, the beam from the light source is homogenized using an engineering diffuser (ED1-C20 Thorlabs, Inc.). The diffuser reshapes the energy distribution into a hat-shape within ± 10 deg. Then, with a telecentric lens and a mirror, the light illuminates the DMD with a uniformity of 95% and a divergence of angle by ± 1.5 deg. With the on/off state of each micromirror, the light is reflected toward or away from the projection optics. The 4:1 projection optics creates a reduced image with a spatial resolution of 1.35 μm. The energy of the light source and the exposure time are set as 74.5 mw and 3 s, respectively. The image is exposed on the image plane which is coated with UV photoresist S1813. This MPLS is currently used for manufacturing the main scale of the absolute optical encoder whose length is 1.5 m. The feature of the periodic grating is about 20 μm with an aspect ratio of 1:1.[18]

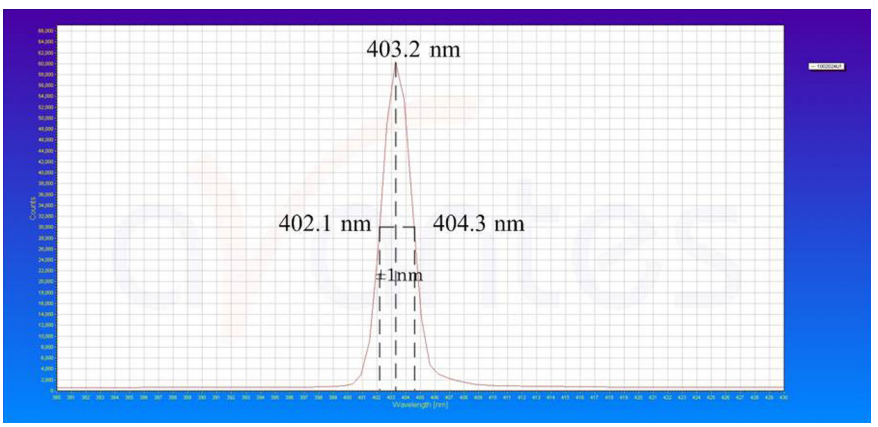

Fig. 8 Spectrogram of the laser source.

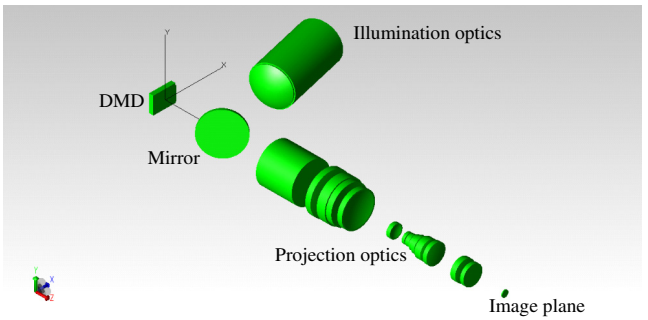

Fig. 11 Diagram of maskless photolithography system in Tracepro.

In the model of MPLS, DMD is the diffraction model as stated in Sec 2.3. Therefore, we set the picture board as a fringe pattern with a period of 20 μm. A +10-μm positive defocusing is used for the image plane. Figure 12(a) gives the simulated result. It is seen that the energy on the left edge is lower than that on the right edge, and the energy on the top edge is higher than that on the bottom edge. This is because defocusing leads to the separation of the diffraction orders. The diffraction efficiencies of (−1, 0) and (0, −1) are lower than those of (1, 0) and (0, 1). Figure 13 gives the schematic of the defocusing effects on energy distribution. With a positive defocusing, the energy on the right edge and on the top edge is higher than that on the left edge and on the bottom edge. If there is negative defocusing, the opposite is true. Therefore, the exposure result in Fig. 12(b) can be explained by the schematic. It can be found that the dots on the right edge are almost connected into a line. On the contrary, the dots on the left edge are separated from each other. The reason for the difference is the energy difference between the two edges which is similar to that of the simulated result in Fig. 12(a). Therefore, we can know that the exposure has a positive defocusing. The dot is a reduced image of each micromirror with 3.34 μm. As the spatial resolution of the projection optics is 1.35 μm, the dot is resolved by the projection optics. According to the result of the analysis above, we can determine the direction of optical focusing by comparison of the energy of the left edge with that of the right edge. Figure 14 shows a simulated

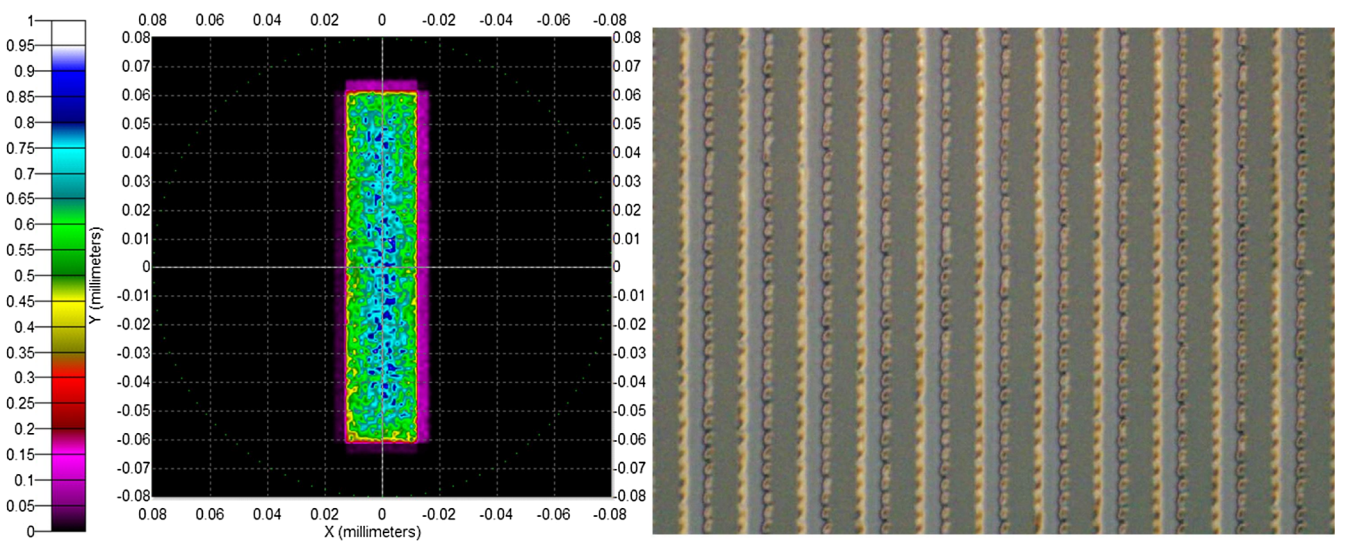

Fig. 12 (a) Energy distribution with defocusing and (b) actual exposure result.

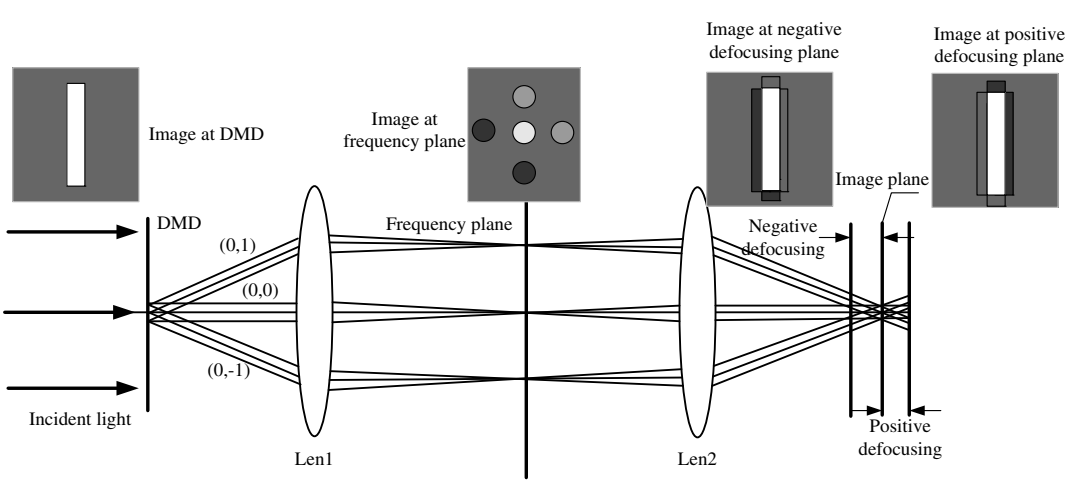

Fig. 13 Schematic of defocusing effect in the system.

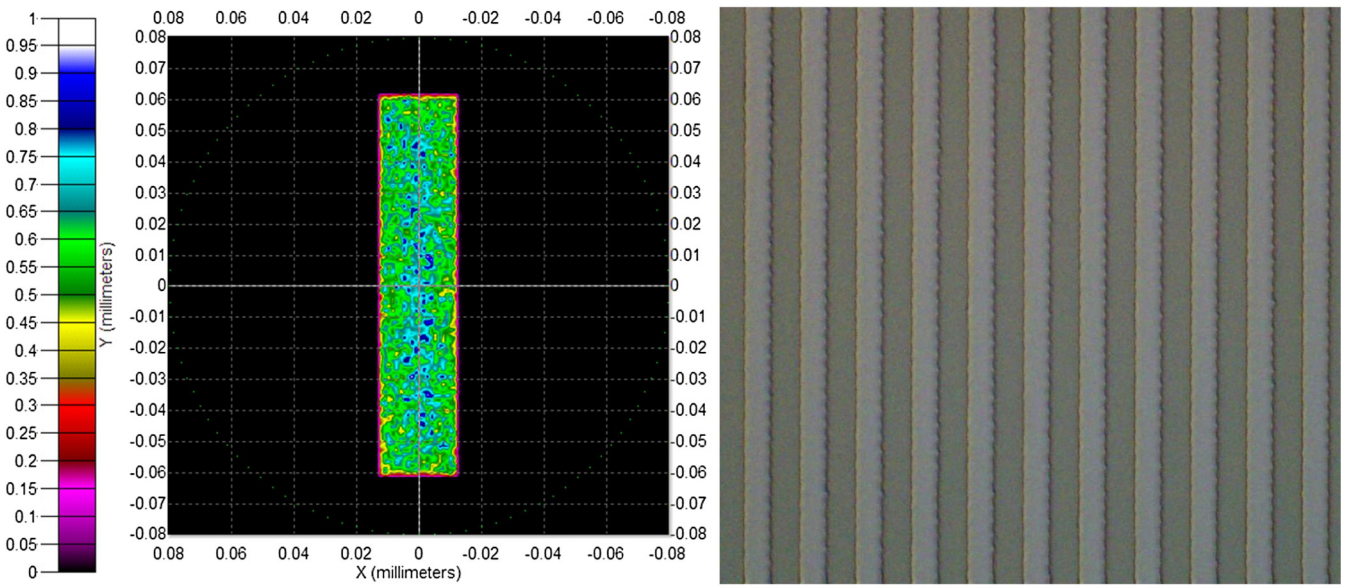

Fig. 14 (a) Energy distribution of image with no defocusing and (b) actual exposure result.

result and an exposure result with no defocusing. The diffraction orders overlap. This result is achieved with the method of energy comparison.

5 Conclusions

In the MPLS, the diffraction property of the DMD is characterized by a numerical model based on Fourier analysis. By using this model, the diffraction efficiency of the DMD is analyzed in terms of the errors of the DMD's manufacture and the precision of the machining of the optical mechanical structure. Results show that the errors, which influence the location of the diffraction envelope, mostly affect the diffraction efficiency. Therefore, it is necessary to have a small tolerance for these errors to limit the variation of the diffraction efficiency to a small amount. Additionally, the diffraction model of the DMD in Tracepro helps us to analyze the degradation of the exposure quality. The difference between the left edge and the right edge of the exposed feature is a result of the separation of the diffraction orders as well as the difference of the diffraction efficiencies. The result of analysis indicates that the direction of optical focusing can be determined by the method of energy comparison of the left edge and the right edge.

Acknowledgments

This work is supported by the National Science and Technology Major Project (No. 2013ZX04007021).

References

1. L. A. Yoder, "The TI digital light processing micromirror tech: putting it to work now," *Adv. Imaging Mag.*, 43–46 (1996).
2. T. G. McDonald and L. A. Yoder, "Digital micromirror devices make projection displays," *Laser Focus World* **33**(8), S5–S8 (1997).
3. D. Dudley, W. Duncan, and J. Slaughter, "Emerging digital micromirror device (DMD) applications," *Proc. SPIE* **4985**, 14–25 (2003).
4. L. V. Wei-Zhen et al., "Design of ultra-thin optical systems in large screen projection display," *Opt. Precis. Eng.* **22**(8), 2020–2025 (2014).
5. J. Y. Son et al., "Holographic display based on a spatial DMD array," *Opt. Lett.* **38**(16), 3173–3176 (2013).
6. P. A. Blanche et al., "Digital micromirror device as a diffractive reconfigurable optical switch for telecommunication," *J. Micro/Nanolith. MEMS MOEMS.* **13**(1), 011104 (2014).
7. X. Chen et al., "Diffraction of digital micromirror device gratings and its effect on properties of tunable fiber lasers," *Appl. Opt.* **51**, 7214–7220 (2012).
8. D. H. Lee, "Optical system with 4 μm resolution for maskless lithography using digital micromirror device," *J. Opt. Soc. Korea* **14**, 266–276 (2010).
9. H. Ryoo, D. W. Kang, and J. W. Hahn, "Analysis of the effective reflectance of digital micromirror devices and process parameters for maskless photolithography," *Microelectron. Eng.* **88**, 235–239 (2011).
10. M. Seo, T. Lee, and H. Kim, "Paramters affecting pattern fidelity and line edge roughness under diffraction effects in optical maskless lithography using digital micromirror device," *Proc. SPIE* **8557**, 855724 (2012).
11. K. J. Kearney and Z. Ninkov, "Characterization of a digital micromirror device for use as an optical mask in imaging and spectroscopy," *Proc. SPIE* **3292**, 81–92 (1998).
12. W. Duncan et al., "DLP switched blaze grating: the heart of optical signal processing," *Proc. SPIE* **4983**, 297–304 (2003).
13. H. Y. Lin and S. C. Chung, "Optical networking by DLP-based switched-blazed-grating," *Proc. SPIE* **5636**, 48–55 (2005).
14. J. P. Rice et al., "DMD diffraction measurements to support design of projectors for test and evaluation of multispectral and hyperspectral imaging sensors," *Proc. SPIE* **7210**, 72100D (2009).
15. "DMD 101: Introduction to digital micromirror device technology," Application Report, DLPA008 (July 2008).
16. T. Kreis, P. Aswendt, and R. Hofling, "Hologram reconstruction using a digital micromirror device," *Opt. Eng.* **40**(6), 926–933 (2001).
17. "DMD 0.7 XGA 12° DDR DMD Discovery," Product Preview Data Sheet, TI DN 2503686 (30 August 2005).
18. L. Hua et al., "Exposure optical system in lithographic main scale of absolute optical encoder," *Opt. Precis. Eng.* **22**(7), 1814–1819 (2014).

Zheng Xiong received his BS degree in optical information science and technology from Changchun University of Science and Technology, China, in 2011. He has been a PhD candidate in optics at the University of Chinese Academy of Sciences since 2012. His current research interests include maskless photolithography systems based on DMD and optical system design.

Hua Liu received her PhD degree in optics from Changchun Institute of Optics, Fine Mechanics and Physics (CIOMP), Chinese Academy of Sciences. She held a postdoctoral position in the State Key Laboratory of Applied Optics at CIOMP. She joined the Optoelectronics Research Center of CIOMP as associate researcher in 2008. Her current research interests include optical design, optical testing, and nonimaging optics.

Xiangquan Tan received his BS and MS degrees in mechanical engineering from Harbin Engineering University, China. He joined the Optoelectronics Research Center of Changchun Institute of Optics, Fine Mechanics and Physics, Chinese Academy of Sciences, as an assistant researcher in 2011. Her current research interests include opto-mechanical systems design and robotic system design.

Zhenwu Lu received his MS degree in optics from Changchun Institute of Optics, Fine Mechanics and Physics (CIOMP), Chinese Academy of Sciences. He is the academic leader of diffraction optics in the State Key Laboratory of Applied Optics at CIOMP. He joined the Optoelectronics Research Center of CIOMP as a researcher in 2008. His current research interests include diffraction optics, optical testing, and nonimaging optics.

Cuixia Li received her BS degree in optical information science and technology from Changchun University of Science and Technology, China, in 2011. She has been PhD candidate in condensed matter physics at the University of Chinese Academy of Sciences since 2011. Her current research interests include upconversion nanoparticle and fiber optical biosensor.

Liwei Song received his MS degree in mechanical engineering from Changchun Institute of Optics, Fine Mechanics and Physics (CIOMP), Chinese Academy of Sciences. He has been a researcher in Changchun Institute of Optics, Fine Mechanics and Physics, Chinese Academy of Sciences. His current research interests include mechanical design and opto-mechanical systems design.

Zhi Wang received his BS and MS degrees in mechanical engineering from Changchun Institute of Optics and Fine Mechanics in 2000 and in 2003, respectively. He received a PhD from Changchun Institute of Optics, Fine Mechanics and Physics (CIOMP), Chinese Academy of Sciences, in 2006. His current research interests include optical system design and optical remote sensing.